Med Bio Eng Comput (2007) 45:35–49
DOI 10.1007/s11517-006-0140-3

ORIGINAL ARTICLE

Snakes based segmentation of the common carotid artery intima media

C. P. Loizou · C. S. Pattichis · M. Pantziaris · T. Tyllis · A. Nicolaides

Received: 11 April 2006 / Accepted: 5 December 2006 / Published online: 3 January 2007

Abstract Ultrasound measurements of the human carotid artery walls are conventionally obtained by manually tracing interfaces between tissue layers. In this study we present a snakes segmentation technique for detecting the intima-media layer of the far wall of the common carotid artery (CCA) in longitudinal ultrasound images, by applying snakes, after normalization, speckle reduction, and normalization and speckle reduction. The proposed technique utilizes an improved snake initialization method, and an improved validation of the segmentation method. We have tested and clinically validated the segmentation technique on 100 longitudinal ultrasound images of the carotid artery based on manual measurements by two vascular experts, and a set of different evaluation criteria based on statistical measures and univariate statistical analysis. The results showed that there was no significant difference between all the snakes segmentation measurements and the manual measurements. For the normalized despeckled images, better snakes segmentation results with an intra-observer error of 0.08, a coefficient of variation of 12.5%, best Bland–Altman plot with smaller differences between experts (0.01, 0.09 for Expert1 and Expert 2, respectively), and a Hausdorff distance of 5.2, were obtained. Therefore, the pre-processing of ultrasound images of the carotid artery with normalization and speckle reduction, followed by the snakes segmentation algorithm can be used successfully in the measurement of IMT complementing the manual measurements. The present results are an expansion of data published earlier as an extended abstract in IFMBE Proceedings (Loizou et al. IEEE Int X Mediterr Conf Medicon Med Biol Eng POS-03 499:1–4, 2004).

Keywords Snakes · Ultrasound imaging · Speckle reduction filtering · Normalization · Carotid artery · Intima media thickness

C. P. Loizou (✉)
Intercollege, Department of Computer Science,
School of Sciences and Engineering, 92 Ayias Phylaxeos Str,
P.O.Box 51604, CY-3507 Limassol, Cyprus
e-mail: christosl@lim.Intercollege.ac.cy

C. S. Pattichis
Department of Computer Science, University of Cyprus,
Nicosia, Cyprus
e-mail: pattichi@ucy.ac.cy

M. Pantziaris · T. Tyllis
Cyprus Institute of Neurology and Genetics,
Nicosia, Cyprus
e-mail: pantziari@cing.ac.cy; tyllisth@cytanet.com.cy

A. Nicolaides
Academic Vascular Surgery, Imperial College, London, UK
e-mail: anicolai@cing.ac.cy

A. Nicolaides
Faculty of Medicine, Division of Surgery,
Anesthetics and Intensive Care, Saint Mary's Hospital,
London, UK
e-mail: anicolai@cing.ac.cy

1 Introduction

The intima media thickness (IMT) of the common carotid artery (CCA) can serve as an early indicator of the development of cardiovascular disease, like myocardial infarction and stroke [3, 15]. Previous studies indicated that increase in the IMT of the CCA is

directly associated with an increased risk of myocardial infarction and stroke, especially in elderly adults without any history of cardiovascular disease [3, 15, 35]. Importantly, increased IMT was demonstrated to have a strong correlation with the presence of atherosclerosis elsewhere in the body and may thus be used as a descriptive index of individual atherosclerosis [15]. As vascular disease develops, local changes occur in arterial structure, which thicken the innermost vessel layers known as intima media complex (IMC). As disease progresses the IMT initially increases diffusely along the artery and then becomes more focal, forming discrete lesions or plaques, which gradually grow and obstruct blood flow. Furthermore, these plaques can become unstable and rupture with debris transported distally by blood to obstruct more distal vessels. This is particular so if plaques develop internal pools of lipid covered only by a thin fibrous cap [3, 15]. In this paper we develop and evaluate a snakes segmentation method for detecting the IMT in ultrasound imaging of the carotid artery after normalisation and speckle reduction filtering.

The use of ultrasound in the diagnosis and assessment of carotid disease is well established because of its non-invasive nature and the continuing improvements in image quality [3, 15]. It provides a non-invasive method for estimating the IMT of human carotid arteries and is specially suited to dynamic analysis owing to its ability to deliver real-time video sequences. A B-mode ultrasound image shown in Fig. 1 shows the IMC at the far wall of the carotid artery, (echo zones Z5–Z6), as a pair of parallel bands, an echodense and an echolucent. The band Z5 and the leading edge of the band Z7 (adventitia) denoted as I5 and I7 define the far-wall IMT. With this understanding, the determination of the IMT at the far wall of the artery becomes equivalent to accurately detecting the leading echo boundaries I5 and I7. The lumen-intima and media-adventitia intensity interface of the far wall of the carotid artery is preferred for IMT measurements [17, 34]. It has been shown that the definition of the IMT as shown in Fig. 1 corresponds to the actual histological IMT [9, 15, 17].

In practice however, detecting the boundaries of the IMC is often complicated and hindered by the presence of ultrasound imaging artefacts, such as speckle, making IMT measurements difficult. Furthermore, the observation of the IMT becomes more difficult as the age of patients increases, due to the presence of acoustic holes (echo-dropouts) in the adventitia layer [15, 35]. The intimal band may appear as a thin low contrast structure and therefore it is difficult to reliably draw boundaries because smoothing can move the structure edges or make them disappear [24]. Traditionally, the IMT is measured by manual delineation of the intima and the adventitia layer [17, 34, 35]. Manual tracing of the lumen diameter (see Fig. 1 Z4) and the IMT (see Fig. 1 I5, I7) by human experts requires substantial experience, it is time consuming and varies according to the training, experience and the subjective judgment of the experts. The manual measurements suffer therefore from considerable inter- and intra-observer variability [17, 34, 35].

Table 1 summarizes various computerized methods that have been developed for vascular ultrasound segmentation of the IMC in carotid artery images. Moreover there are a few known commercial software-imaging systems supporting IMC segmentation made available from different research groups [6, 34], which are based on snakes [6] and on dynamic programming segmentation [34].

The problems that are associated with the computer-assisted border tracing segmentation procedures (also presented in Table 1) are the following: (1) They do not take into consideration the speckle noise or the image normalization in the ultrasound image [24]. (2) They are sensitive to the initial snake contour [6], or initial seed points, which need to be placed manually

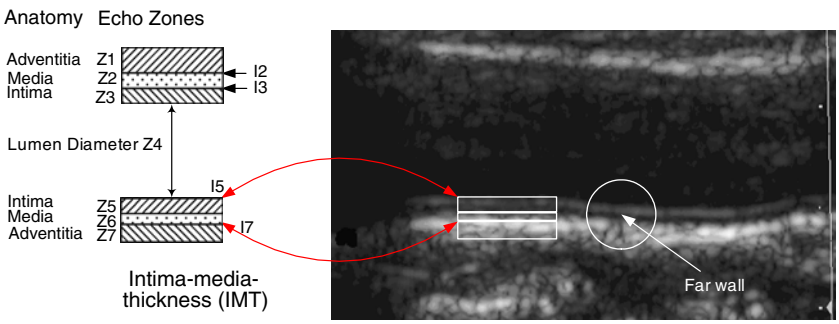

Fig. 1 Illustration of the intima-media-complex (*IMC*) of the far wall of the common carotid artery. The IMC consists of the intima band (Z5), the media band (Z6) and the far wall adventitia band (Z7). The IMT complex is defined as the distance between the blood intima interface line and the media adventitia interface line. See also [17]

Table 1 An overview of IMC segmentation techniques in ultrasound imaging of the carotid artery

Segmentation technique	Year	Input	2D/3D	AIC	UI	MC	IMT_{mean} (mm)	*N*
Dynamic programming [34] with cost function optimization	1997	USC	2D	No	Yes	Yes	0.93	69
Texture based [24]	1997	IVUS	2D	–	Yes	No	0.68	29
Multiscale dynamic programming [17]	2000	USC	2D	No	Yes	Yes	0.92	50
Discrete dynamic contour [23]	2000	USC	2D	No	Yes	No	–	7
Deformable model [40]	2001	USC	3D	Yes	Yes	Yes	–	69
Edge-tracking [29]	2001	USC	2D	No	Yes	Yes	0.78	24
Snakes [6]	2002	USC	2D	Yes	Yes	Yes	0.65	32
Gradient based [30]	2005	USC	2D	Yes	Yes	Yes	0.7	50

US Ultrasound images, *USC* ultrasound carotid images, *IVUS* intra vascular ultrasound, *AIC* automatic initial contour, *UI* user interaction, *MC* manual correction possible, IMT_{mean} mean IMT in mm, *N* number of subjects investigated

[40]. If the initial contour is placed far away from the boundary of interest then the snake will not be attracted [6]. (3) Some weighting factors that should be tuned due to the varied characteristics of the ultrasound instrumentation must be entered manually or empirically [24, 34, 37, 40]. Some other weights may be adjusted by a training procedure, which might be long and requires experts tracing [17, 23]. (4) The snake is implemented as a close contour [8, 36, 40] that might not be that suitable for the IMC segmentation. (5) They require manual correction after automatic tracing [6, 23, 24, 34]. (6) In a number of cases there was no ground truth segmentation delineations from experts to compare to the computer assisted methods [6, 24]. (7) Different measurement procedures were used between the manual and the snakes segmentation methodologies (see Fig. 1, [6, 17, 23, 34]). (8) Different criteria were used for assessing the performance of the segmentation algorithms [6, 40]. (9) They were evaluated on a limited number of images, where the intra- and inter-observer variability could not be assessed [23, 37].

The objective of this paper was to develop, and evaluate an IMC snakes segmentation method, by utilizing an improved snake initialization method, and an improved validation of the segmentation method, based on the Williams and Shah snake [36]. The snakes segmentation method also utilizes image normalization and speckle reduction in ultrasound images of the carotid artery trying to overcome some of the above difficulties. Furthermore, to investigate under what conditions the snakes segmentation measurements are closer to the manual segmentation measurements. Preliminary results of this study were also published in [19].

2 Materials and methods

2.1 Recording of ultrasound images

A total of 100 B-mode longitudinal ultrasound images of the CCA used for the IMC segmentation, were acquired by the ATL HDI-3000 ultrasound scanner (Advanced Technology Laboratories, Seattle, USA). The ATL HDI-3000 ultrasound scanner is equipped with 64 elements fine pitch high-resolution, 38 mm broadband array, a multi element ultrasound scan head with an operating frequency range of 4–7 MHz, an acoustic aperture of 10×8 mm and a transmission focal range of 0.8–11 cm. Digital images were resized using the bicubic method to standard pixel density of 16.66 pixels/mm. This was carried out due to the small variations in the number of pixels per mm of image depth (i.e. for deeply situated carotid arteries, image depth was increased and therefore digital image spatial resolution would have decreased) and in order to maintain uniformity in the digital image spatial resolution [14]. The images were logarithmically compressed and were recorded digitally on a magneto optical drive at size of 768×576 pixels with 256 grey levels.

The images were recorded at the Cyprus Institute of Neurology and Genetics, in Nicosia, Cyprus, from 42 female and 58 male symptomatic patients aged between 26 and 95 years old, with a mean age of 54 years. These subjects were at risk of atherosclerosis and have already developed clinical symptoms, such as a stroke or a transient ischemic attack.

2.2 Image normalization

Brightness adjustments of ultrasound images were carried out in this study based on the method introduced in [9]. It was shown that this method improves image compatibility by reducing the variability introduced by different gain settings, different operators, different equipment and facilitates ultrasound tissue comparability [9, 31]. Algebraic (linear) scaling of the image was performed by linearly adjusting the image so that the median grey level value of the blood was 0–5, and the median grey level of the adventitia (artery wall) was 180–190 [9]. The scale of the grey level of the

images ranged from 0 to 255. Thus the brightness of all pixels in the image was readjusted according to the linear scale defined by selecting the two reference regions. It is noted that a key point to maintaining a high reproducibility was to ensure that the ultrasound beam was at right angles to the adventitia, adventitia was visible adjacent to the plaque and that for image normalization a standard sample consisting of the half of the width of the brightest area of adventitia was obtained.

2.3 Speckle reduction

The leading edge of the adventitia Z7 (I7, and the Media layer Z6) is affected due to speckle noise and the attenuation of the probing sound wave by sound absorbing tissues [1, 19]. The texture is not homogeneous, the intensity values vary and the boundary is incomplete. Therefore it is important to despeckle the area of interest prior to segmentation.

In this study, a linear scaling filter (*lsmv*) utilizing the mean and the variance of a pixel neighbourhood was used. This filter was introduced by [16], and evaluated on ultrasound imaging of the carotid artery giving best results in [18]. The *lsmv* filter may be described by a weighted average calculation using sub region statistics to estimate statistical measurements over 7×7 pixel windows [16, 18]. The filter was applied iteratively five times on each image as documented in [18].

2.4 Manual measurements and visual perception evaluation

Although the power Doppler (blood flow image) was found to be useful for locating the lumen, only the B-mode image was used when delineating the wall and lumen boundaries in order to eliminate errors due to colour artefacts and verberations occurring from the blood flow image [9, 20, 27]. For the purpose of this study the vessel wall and lumen are defined as follows: (1) The lumen is the area through which blood flows (see Fig. 1, Z4). (2) The lumen appears as a dark region in a B-mode image (see Fig. 1, region between interfaces Z3–Z5). (3) The vessel wall is the boundary separating the intima-blood interface (see Fig. 1 interface Z5). (4) The intima media interface is frequently visible except in cases where artefacts may obscure visualization of this boundary (see Fig. 1, interfaces Z5–Z7). (5) On longitudinal images, the IMT and the vessel wall are always defined as a pair of two contours, which may be represented by a cubic spline.

The two vascular experts delineated manually (using the mouse) the IMT on 100 longitudinal ultrasound images of the carotid artery before and after image normalization (see Sect. 2.2) by selecting 20–40 consecutive points for the adventitia and the intima at the far wall of the CCA. The manual delineations were performed using a system implemented in MATLAB from our group. The measurements were performed between 1 and 2 cm proximal to the bifurcation of the CCA on the far wall [27] over a distance of 1.5 cm starting at a point 0.5 cm and finishing at a point 2.0 cm proximal to the carotid bifurcation. The bifurcation of the CCA was used as a guide and all measurements made from that region. The IMT was then calculated as the average of all the measurements. The measuring points and delineations were saved for comparison with the snakes segmentation method. Two sets of measurements were carried out by both experts with a 12 months interval. All sets of manual segmentation measurements were performed by the two experts in a blinded manner, both with respect to identifying the subject and as to the image delineation.

2.5 IMT initialization

It is important to place the initial snake contour as close as possible to the area of interest otherwise the snake may be trapped in local minima or false edges, and converge to a wrong location. The initial contour selection and the convergence are two of the main limitations of the snake models proposed in the literature [4, 6, 13, 34, 37, 40].

The initialization procedure proposed in this study may be described as follows (see Fig. 2):

1. Load the initial B-mode image, and select using the mouse the area of interest on the image, where the IMT will be detected. The area may be drawn around the IMT borders (see Fig. 2a).
2. The selected cropped area is shown in Fig. 2b.
3. Despeckle the selected area by applying the *lsmv* filter presented in Sect. 2.3 (see Fig. 2c).
4. Convert the area to binary by image thresholding, in order to extract edges more easily (see Fig. 2d). A threshold is calculated from the despeckled grayscale image according to [26]. The threshold is chosen so that the intraclass variance [26] of the thresholded black and white pixels is minimized. It should be noted that the cropped out area expresses a bimodal histogram distribution. The threshold is then applied to all the pixels in the image. Pixels

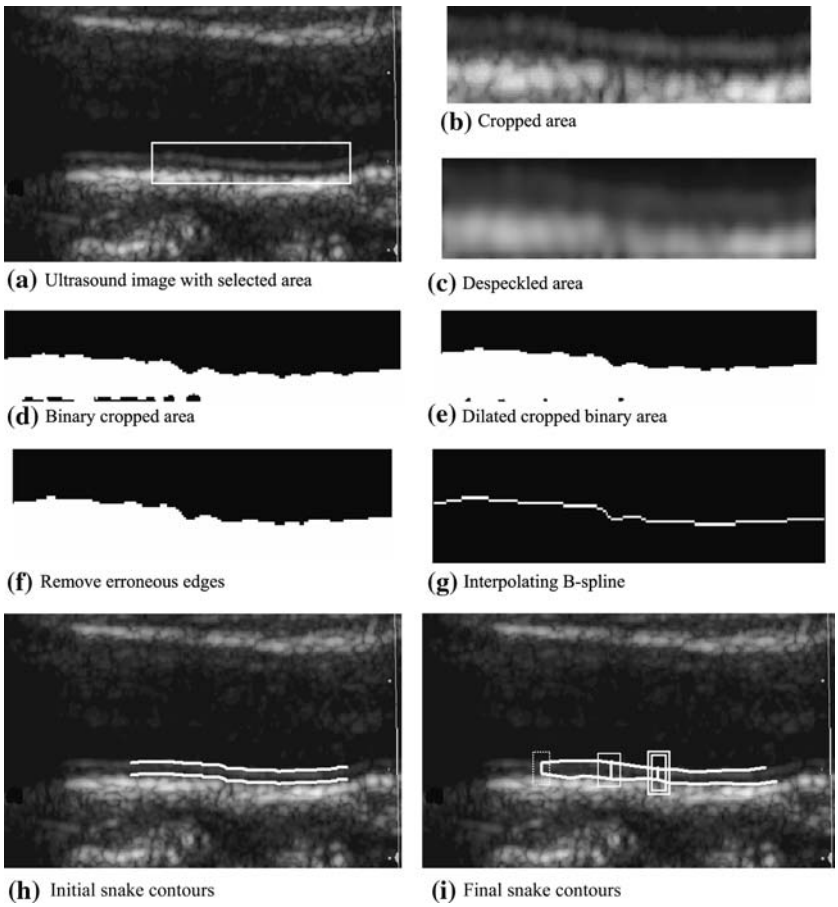

Fig. 2 **a** Original ultrasound image with selected area, **b** cropped area, **c** despeckled area, **d** binary cropped area, **e** dilated cropped area, **f** dilated area after removal of small edges, **g** construction of the interpolating B-spline, **h** detected initial contours for the adventitia and the intima layers, **i** final contours after the snake deformation. The IMT_{mean}, is shown with *full line box*, the IMT_{max}, with a *dashed line box* and the IMT_{min}, with *double line box*

that have smaller intensity values than this threshold are set to zero, whereas pixels with larger intensity values are set to one.

5. Dilate the binary image (from point (4) above) by a 3×3 pixel-structuring element consisting of ones, which is multiplied with the binary image. This morphological operation is performed to close small gaps and form a continuous boundary (see Fig. 2e).
6. Remove erroneous small edges that might trap the snake. This is carried out by labelling connecting components in the image where the number of connecting components in a pixel neighbourhood was chosen to be 8. Small segments that are smaller than 20 pixels, and do not belong in the boundary are therefore removed (see Fig. 2f).
7. Extract the contour matrix of the above area (see Fig. 2f) by locating points and their coordinates on the adventitia (contour) and construct an interpolating B-spline (see Fig. 2g). Sample the interpolating B-spline, in equal distance points, in order to define a number of snake elements on the contour. The number of snake points was variable and was determined according to the area chosen by the user (see Fig. 2a). The number of snake points was estimated by dividing the number of pixels belonging to the largest size of the area defined in Fig. 2a, by 30. This will affect that fewer or more snake points will be defined for a smaller or a larger area, respectively.
8. Map the detected contour points from g), on the B-mode image of Fig. 2a, to form the initial snake contour for the adventitia (see Fig. 2h). Displace the initial contour estimate of point g) for the adventitia, upwards for up to 17 pixels (1.02 mm) to form the initial snake contour for the intima layer. This displacement is based on the observation that the IMT lies between 0.6 and 1.4 mm (0.6 mm < IMT < 1.4 mm), with a mean IMT of 1.0 mm [34]. By taking into consideration that the spatial resolution (distance between 2 pixels) is 0.06 mm, then the IMT is lying within the range of 10 < IMT < 24 pixels, with a mean of 17 pixels. Therefore the displacement of the contour, in order to estimate the intima should be in average 17 pixels

(1.02 mm) upwards. Figure 2h shows the initial contour estimation for the adventitia and the intima layers as they have been detected by the initialization technique.

Apply the snakes segmentation algorithm (see Sect. 2.6) to extract the final snake contours (see Fig. 2i), and carry out the IMT measurements.

2.6 IMC segmentation

The snakes segmentation technique implemented in this study is based on an energy function as defined by Williams and Shah [36], which is an extension of the initial snake functional defined by Kass et al. [13]. An additional image energy term, E_{image} (v) [38], which is given by the negative gradient of the current contour point $g_{i,j}$ as E_{image} $(v) = -\nabla g_{i,j}{}^2$, was added to our energy functional, as also proposed in [39]. For the calculation of the snake parameters, $\alpha(s)$, and $\beta(s)$, we took into consideration the irregular spacing between the contour points of the snake and were calculated as proposed in [7]. We have chosen in our study the initial values of $\alpha_i(s) = 0.6$, $\beta_i(s) = 0.4$ and $\gamma_i(s) = 2$, to start the snake deformation, which is consistent with other studies [6, 33, 39].

The extracted final snake contours (see Fig. 2i), correspond to the leading echo boundaries I5 and I7. The distance is computed between the leading echo boundaries I5 and I7, at all points along the arterial segment of interest moving perpendicularly between pixel pairs, and then averaged to obtain the mean IMT (IMT_{mean}). Also the maximum (IMT_{max}), minimum (IMT_{min}) and median ($\text{IMT}_{\text{median}}$) IMT values, are calculated, displayed and plotted on the B-mode image. Figure 2i shows the detected IMT_{mean}, IMT_{max} and IMT_{min} values with a double line box, full line box and a dashed line box, respectively.

2.7 Univariate statistical analysis

In order to investigate how the results of the snakes segmentation method differ from the manual delineation results, we used the following evaluation metrics.

We computed the parameters IMT_{mean}, IMT_{min} IMT_{max} and $\text{IMT}_{\text{median}}$, as well as the intra-observer error [17, 34] according to the formula $\text{se} = \sigma_{\text{IMT}}\sqrt{2}$, with, σ_{IMT}, the standard deviation for each 100 measurements. We also calculated the coefficient of variation, CV%, which describes the difference as a percentage of the pooled mean value with $\text{CV}\% = \frac{\text{se}}{\text{IMT}}100$ [17, 34].

The Wilcoxon matched pairs rank sum test was used in order to identify if for each set of measurements a significant difference (S) or not (NS) exists between all segmented boundaries, at $p < 0.05$.

Furthermore a variation of the Hausdorff distance, HD, [5] between two curves was calculated. It reflects the maximum mismatch (HD = Manual – Snakes_Segmented between the manual and the snakes segmented areas, where small values for the HD are favorable.

These statistical metrics have been computed for the Williams and Shah snakes segmentation measurements for the cases, no pre-processing (NP), despeckled (DS), normalized (N), normalized despeckled (NDS) and for the manual segmentation measurements, for the cases, manual no preprocessing (NP) and manual normalized (N) from both experts, respectively. Additionally, in order to assess the intra-observer variability between the two experts, the manual measurements on original (NP), and normalized (N) images were repeated from both experts, 1 year after the first measurements.

Bland–Altman plots [2], with 95% confidence intervals, were also used to further evaluate the agreement between the Williams and Shah snakes segmentation and the manual segmentation method. The plots were investigated for the snakes segmentation cases, NP, DS, N, NDS, and for the manual segmentation cases from both experts. By using Bland–Altman plots, the distributions of the differences between all different cases were computed.

3 Results

3.1 An example of IMC segmentation

Figure 3a shows a longitudinal ultrasound image of the carotid artery with the manual delineations from the two experts (Fig. 3b, c), the automatic initial contour estimation (Fig. 3d), and the Williams and Shah snakes segmentation results for the cases of no pre-processing (NP) (Fig. 3e), despeckled (DS) (Fig. 3f), normalized (N) (Fig. 3g), and normalized despeckled (NDS) (Fig. 3h). The detected IMT_{mean}, IMT_{max} and IMT_{min} values, are shown with a double, single and dashed line boxes, respectively.

The manual measurements are given for each expert, in cases when manual measurements were carried out, without normalization (NP) and with normalization (N). The Williams and Shah snakes segmentation measurements are given for the NP, DS, N and NDS cases, and were in most of the cases, higher than the manual measurements, except in the N case for both experts. The observed standard deviation, sd, values for the IMT_{mean}, was for the first expert NP (0.14), N

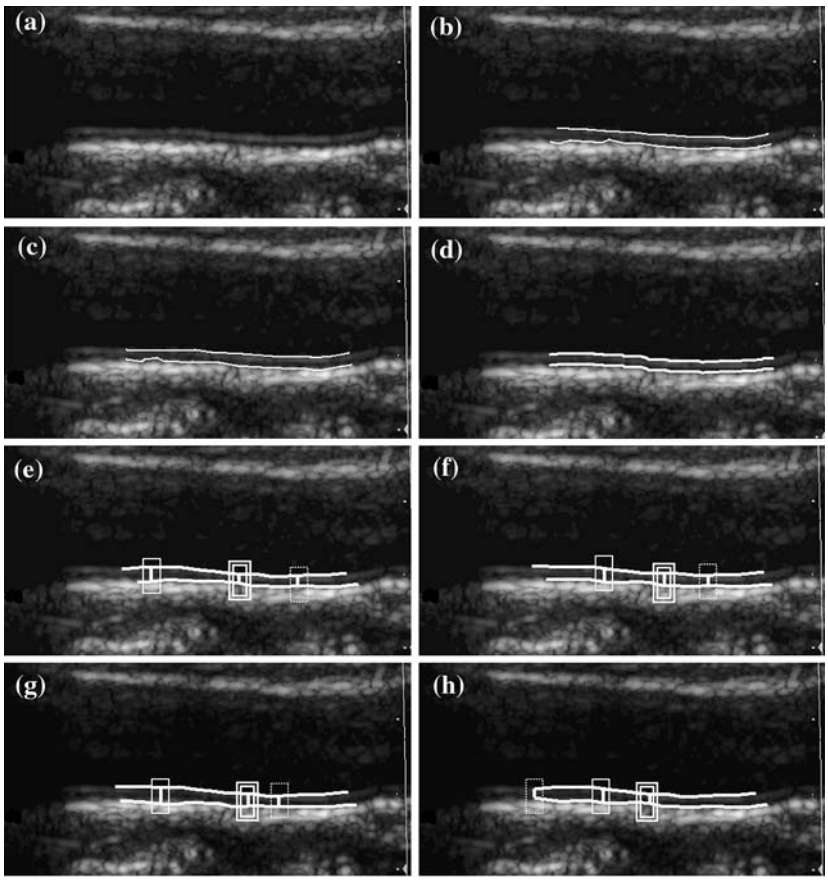

Fig. 3 **a** Original longitudinal ultrasound image of the carotid artery, **b** manual delineation from Expert 1, **c** manual delineation from Expert 2, **d** initial contour estimation, and the segmentation results of the IMC for, **e** no pre-processing (*NP*), **f** despeckled (*DS*), **g** normalized (*N*), and **h** normalized despeckled (*NDS*) images. The detected IMT_{mean}, IMT_{max} and IMT_{min} are shown with a *single*, *dashed* and *double line boxes*, respectively

(0.11), for the second expert NP (0.12), N (0.15), and for the snakes segmentation NP (0.24), DS (0.20), N (0.17) and NDS (0.19), respectively. The results in Fig. 3 showed, that the IMT was detected in all snakes segmentation measurements but with variations between experts and methods.

3.2 Univariate statistical analysis

Table 2 tabulates the first set of manual and the Williams and Shah snakes segmentation results for 100 longitudinal ultrasound images of the carotid artery, for the IMT_{mean}, IMT_{min}, IMT_{max} and IMT_{median}, with their sd, se and CV%. The $IMT_{mean} \pm$ sd results for Expert 1 were, 0.67 ± 0.16 mm, 0.68 ± 0.17 mm, and for Expert 2 were, 0.65 ± 0.18 mm, 0.61 ± 0.17 mm on the NP and N images, respectively. The $IMT_{mean} \pm$ sd snakes segmentation results were 0.7 ± 0.14, 0.69 ± 0.13, 0.67 ± 0.13 and 0.68 ± 0.12 mm, for the NP, DS, N and NDS, images respectively.

The middle part of Table 2 presents the second set of manual measurements for the 100 images of the carotid artery made by the two experts 12 months after the first set of measurements were made. This was carried out in order to assess the intra-observer variability for the same expert. It is shown that the measurements made by Expert 2 are generally smaller giving a thinner IMT. Furthermore, the sd, the se and the CV%, for the measurements made by Expert 2 are also smaller.

Table 3 presents the results for the Wilcoxon rank sum test for all manual segmentation, measurements. It is shown that the measurements made by the two experts on the N images are mostly NS, whereas the measurements on the NP images before normalization demonstrated a higher number of significant difference measurements. More specifically, the manual measurements of Expert 1 at time 0 versus time 12 months were S, whereas the measurements of Expert 1 at time 0 versus Expert 2 at time 12 months were S for the NP and NS for N. The measurements of Expert 2 at time 0 versus the measurements of Expert 1 and Expert 2 at 12 months and the measurements of Expert 1 versus Expert 2 at time 12 months were all NS.

Table 4 shows the results of the Wilcoxon rank sum test, and a variation of the HD between Expert 1 and Expert 2 and the snakes segmentation measurements. The Wilcoxon rank sum test, which is displayed in the

Table 2 Comparison between manual and snakes segmentation measurements for the 100 ultrasound images of the carotid artery

	Manual first set of measurements at time 0				Manual second set of measurements at time 12 months				Snakes segmentation measurements			
	Expert 1		Expert 2		Expert 1		Expert 2					
	NP	N	NP	N	NP	N	NP	N	NP	DS	N	NDS
IMT_{mean} (sd)	0.67 (0.16)	0.68 (0.17)	0.65 (0.18)	0.61 (0.17)	0.67 (0.16)	0.68 (0.17)	0.55 (0.11)	0.57 (0.13)	0.70 (0.14)	0.69 (0.13)	0.67 (0.13)	0.68 (**0.12**)
IMT_{min} (sd)	0.53 (0.14)	0.52 (0.15)	0.57 (0.16)	0.54 (0.14)	0.53 (0.14)	0.52 (0.15)	0.45 (0.11)	0.47 (0.14)	0.51 (0.13)	0.51 (0.13)	0.51 (0.14)	0.49 (**0.11**)
IMT_{max} (sd)	0.82 (0.22)	0.85 (0.21)	0.75 (0.19)	0.70 (0.20)	0.82 (0.22)	0.85 (0.21)	0.64 (0.13)	0.66 (0.14)	0.90 (0.20)	0.88 (0.19)	0.86 (0.17)	0.87 (**0.15**)
IMT_{median} (sd)	0.66 (0.16)	0.66 (0.18)	0.67 (0.18)	0.61 (0.17)	0.66 (0.16)	0.66 (0.18)	0.62 (0.16)	0.61 (0.14)	0.69 (0.14)	0.69 (0.13)	0.66 (0.12)	0.64 (**0.12**)
se	0.11	0.12	0.13	0.11	0.11	0.12	0.08	0.1	0.10	0.09	0.09	**0.08**
CV%	16.7	17.1	19.1	17.2	16.7	17.1	14.0	16.8	13.8	13.4	13.2	**12.5**

Measurements are in millimeters (mm). Bolded values show best performance

NP No pre-processing, *N* normalized, *DS* despeckled, *NDS* normalized despeckled, *sd* standard deviation, *se* intra-observer error for mean values, *CV%* coefficient of variation

Table 3 Comparison of all IMT manual segmentation measurements based on the Wilcoxon ranksum test

			First set of manual measurements at time 0				Second set of measurements at time 12 months			
			Expert 1		Expert 2		Expert 1		Expert 2	
			NP	N	NP	N	NP	N	NP	N
First set of manual measurements at time 0 months	Expert 1	NP					S (0.01)	S (0.01)	S (0.0)	NS (0.2)
		N	S (0.04)				S (0.00)	S (0.00)	S (0.00)	NS (0.47)
	Expert 2	NP	S (0.03)	NS (0.07)			NS (0.45)	NS (0.07)	NS (0.2)	NS (0.09)
		N	S (0.00)	NS (0.09)	NS (0.45)		NS (0.87)	NS (0.06)	NS (0.55)	NS (0.09)
Second set of manual measurements at time 12 months	Expert 1	NP						S (0.0)	NS (0.06)	NS (0.07)
		N							NS (0.47)	NS (0.07)
	Expert 2	NP								NS (0.54)
		N								

NP No pre-processing, *N* normalzed. The *p* value is also shown in parentheses (*S* Significant difference at $p < 0.05$, *NS* non significant difference at $p > 0.05$)

Table 4 Tests and measures computed on 100 ultrasound images of the carotid artery from Expert 1 and Expert 2 and the snakes segmentation measurements

		Wilcoxon ranksum test and HD													
		First set manual Expert 1			Automated				First set manual Expert 2			Automated			
		NP	N	Ex-	NP	DS	N	NDS		NP	N	Ex-	NP	DS	N	NDS
First set manual Expert 1, Expert 2	NP	–	–		NS (0.45)	NS (0.56)	NS (0.64)	NS (0.9)	NP	–	–		NS (0.06)	NS (0.1)	NS (0.07)	NS (0.09)
	N	13.3	–		NS (0.90)	NS (0.79)	NS (0.30)	NS (0.55)	N	40	–		NS (0.08)	NS (0.07)	NS (0.1)	NS (0.16)
	NP	27.1	13.8		–	NS (0.87)	NS (0.33)	NS (0.53)	NP	46.2	86.2		–	NS (0.87)	NS (0.33)	NS (0.53)
Automated	DS	21.9	**8.6**		**5.2**	–	NS (0.45)	NS (0.69)	DS	41	81		**5.2**	–	NS (0.41)	NS (0.55)
	N	**3.4**	9.9		23.7	19	–	NS (0.41)	N	22.5	62.5		23.7	19	–	NS (0.69)
	NDS	**8.6**	**4.7**		18.5	13	**5**	–	NDS	27.7	67.7		18.5	13	**5**	–

Left and right columns upper triangle: Wilcoxon ranksum test with the p value shown in parentheses. Left and right columns lower triangle: Variation of the Hausdorff distance ($*10^{-3}$ mm). Bolded values show best performance

NP No pre-processing, *N* normalized, *DS* despeckled, *NDS* normalized despeckled, The p value is also shown in parentheses (*S* Significant difference at $p < 0.05$, *NS* non significant difference at $p > 0.05$)

upper triangle of the left and right columns of Table 4, showed that NS difference existed between the Williams and Shah snakes segmentation measurements and the manual measurements from Expert 1 and Expert 2, respectively. The NS difference between the two methods showed that the manual measurements may be replaced by the snakes segmentation measurements with confidence. The HD displayed in the left and right columns lower triangle of Table 4, showed that minimum mismatches were obtained for Expert 1, between the N-Manual first set NP (3.4), NDS-Manual first set N (4.7), NDS-N (5), DS-NP (5.2), NDS-Manual first set NP and DS-Manual first set N (8.6), and for Expert 2 between the NDS-N (5), and DS-NP (5.2) respectively.

Figure 4 presents the histogram distributions for the IMT_{mean} values for all 100 ultrasound images of the carotid artery for the cases, manual (first set of manual measurements from both experts on the original, NP, and normalized, N, images), and automated (NP, DS, N and NDS) measurements respectively. Statistical tests performed showed that all the histograms of the IMT_{mean} can be fitted to a Rician distribution. The IMT manual measurements showed a high variability between the first and the second set of measurements for each expert and between them.

Figure 5 illustrates a Bland–Altman plot between the first set of manual normalized measurements of Expert 1 (N) and the NDS segmentation methods. For both experts the best plots were obtained for the NDS images where the difference with the segmentation method for the manual measurements ± the standard deviation of Expert 1, was –0.01 + 0.24 and –0.01 to 0.25 (see also Fig. 5), and for the manual normalized measurements of Expert 2, was 0.09 + 0.3 and 0.09 – 0.13.

Figure 6 presents the results of the IMT_{mean} values versus age using regression analysis. It is shown that the IMT_{mean} increases almost linearly with increasing age. Furthermore, it is shown that the IMT_{mean}, at the age of 60.5 is 0.67 mm. Figure 6 also shows that the confidence interval limits for the IMT_{mean}, are ±0.24 mm. Furthermore, it is shown in this study that the values of the IMT in a normal carotid artery may vary between 0.4 and 1.0 mm, depending on age, and this is also consistent with other studies [11].

4 Discussion

The objective of this paper was to develop, and evaluate an IMC snakes segmentation method, by utilizing an improved snake initialization method, and an improved validation of the segmentation method, based

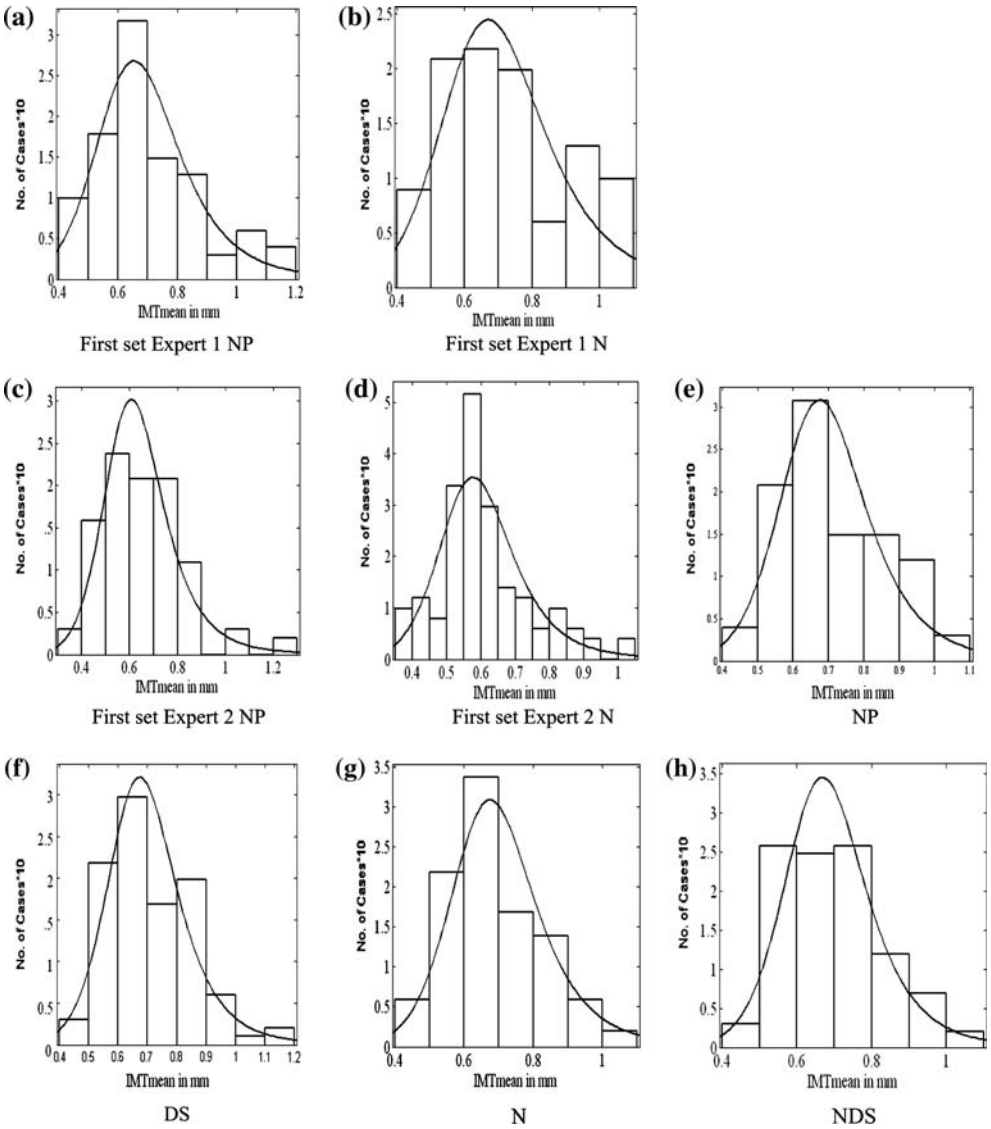

Fig. 4 Histograms of the IMT_{mean} values for the: **a** manual first set of measurements from Expert 1 (NP), **b** manual normalized first set of measurements from Expert 1 (N), **c** manual first set of measurements from Expert 2 (NP), **d** manual normalized first set of measurements from Expert 2 (N), **e** no pre-processing (NP), **f** despeckle (DS), **g** normalized (*N*), and **h** normalized despeckled (*NDS*), images

on the Williams and Shah snake. The snake segmentation method also utilizes image normalization and speckle reduction in ultrasound images of the carotid artery. Furthermore, to investigate under what conditions the snakes segmentation measurements are closer to the manual segmentation measurements.

The study showed (see Table 2) that the manual IMT measurements have a larger range of values whereas the snakes segmentation measurements were more concentrated for all cases NP, DS, N, NDS. Similar IMT findings were also reported in [12, 34].

Initial contour estimation was proposed in this work where some of the limitations of this method were outlined in Sect. 2.5. Cheng et al. [6] proposed an IMT segmentation method where the starting and endpoints of the snake must be defined by the user. A dynamic programming segmentation method using a cost function proposed in [17], utilized an initial contour estimation method for segmenting transversal carotid artery images. Initial contour estimation was also proposed in [23], which was derived from the entropy image using an initial circle matching procedure. In [40] a geometrically deformable model was initialized by manually placing a seed point in the centre of the lumen for segmenting the lumen in 3D carotid artery images. In all of these studies as well as in the present study, the significance of the initial contour placement was not investigated in order to estimate how this influences the final segmentation result.

To the best of our knowledge no other study carried out ultrasound image normalization, as described in this study, prior to segmentation of the IMT. However, in [24], histogram equalization was performed on carotid artery ultrasound images for increasing the image

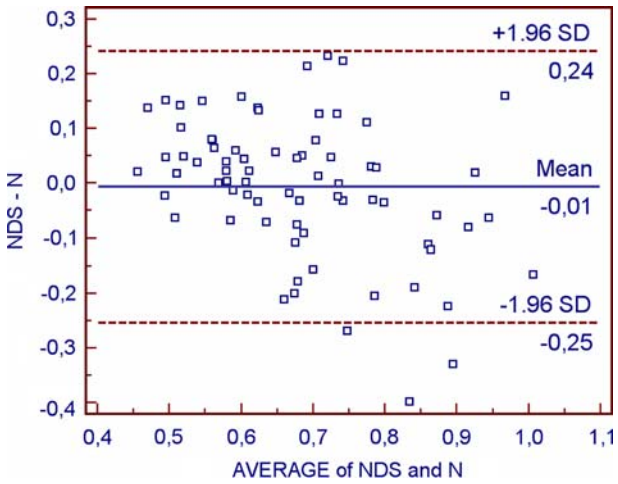

Fig. 5 Regression lines (Bland–Altman plots) of manual versus Williams and Shah snakes segmentation method for the IMT_{mean} between the first set of manual normalized (N) measurements of Expert 1 and NDS. The *middle line* represents the mean difference, and the upper and lower two outside lines represent the limits of agreement between the two methods, which are the mean of the data ±2sd for the estimated difference between the two methods

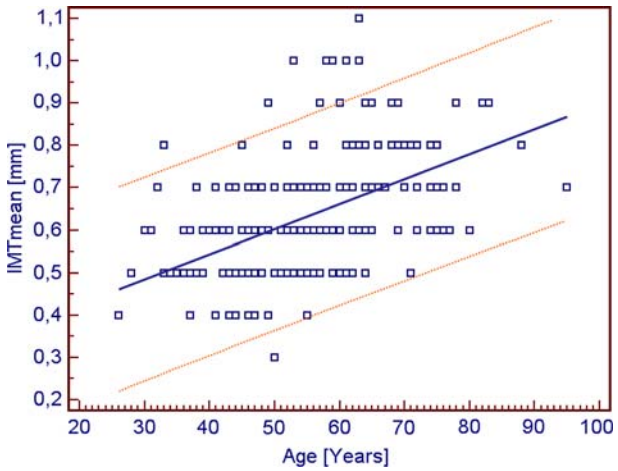

Fig. 6 Increase of IMT_{mean} with age, with confidence interval limits ±0.24 mm

contrast. The normalization method used in this study was documented to be helpful in the manual contour extraction [21] as well as the snakes segmentation of the IMT [19]. Moreover, this method increased the classification accuracy of different plaque types as assessed by the experts [25].

In this paper speckle reduction filtering was used as a pre-processing step based on our previous work [18] where it was shown that this improves the image quality and the visual evaluation of the image [21]. Speckle reduction filtering of the carotid artery was also applied in [1], where it was also shown that this improves the image quality and visual interpretation of the experts. More, specifically, in [18], it was shown that image normalization followed by speckle reduction filtering produces better quality images, whereas the reverse (speckle reduction filtering followed by normalization) might produce distorted edges. The preferred method is to apply first normalization and then speckle reduction filtering for better results. Speckle reduction filtering of the carotid was also proposed by [19–21] where it was shown that this improves the image quality and the visual evaluation of the image. However, in other segmentation studies for extracting the carotid artery plaque borders in IVUS imaging, speckle was used as useful information [5, 6, 23, 24, 32, 34, 37, 40].

The smaller CV% (12.5%), as well as the smaller se (0.08), in Table 2, for the NDS images, showed that the Williams and Shah snakes segmentation method, is more reproducible when performed on the NDS images. The manual measurements reported in this study (0.67, 0.68, 0.65 and 0.61 mm for Expert 1 and Expert 2 with, N, and without, NP, normalisation) were smaller than the snakes segmented, and this finding was also reported in other studies. Specifically, the manual versus the snakes segmented IMT measurements reported in other studies were (0.88 vs. 0.93 mm) [17], (0.88 vs. 0.92 mm) [34], and (0.63 vs. 0.72 mm) [12]. For both experts the Williams and Shah snakes segmentation method gave higher values for the IMT compared with the manual measurements as shown in Table 2. There is a large variation in the IMT measurements between the studies reported above and this study. This is due to the fact that the sample of images used in this study was mainly taken from symptomatic patients at the early stages of the atherosclerosis disease.

The CV%, of this study when compared to other studies [5, 12, 17, 34] was higher for the manual measurements, but lower for the snakes segmentation measurements, which were performed on the NDS images. Specifically in [12], a CV% = 14% was reported for the manual measurements made on 30 ultrasound longitudinal images of the carotid artery, whereas a CV% = 12.8%, was reported for the active contour snakes segmentation measurements improved by multi-resolution analysis. Selzer et al. [29] performed a study for measuring automatically the IMT on 24 healthy randomly selected subjects and reported a CV% of 4.03 and 3.46% for the IMT measured at maximum and minimum diameter of the carotid artery respectively. In another study Stein et al. [30], developed and tested a gradient based semi-automated

border detection technique on 50 carotid artery ultrasound images and reported a CV% for 5.4 and 3.4% for the manual and the automated methods respectively. In the studies reported above, i.e. [5, 12, 17, 29, 30, 36, 37, 40] no despeckle filtering and image normalization was carried out as performed in this study.

The results from Table 2 showed that high intra observer variabilities occur when manual measurements are made. It is documented in the literature that measurements of the *se*, can be used as clinically useful standard to measure the performance of image segmentation algorithms [5]. There are some results given in the literature for the intra observer variability for the IMC segmentation performed in carotid artery images. Specifically, in [32] the $IMT_{mean} \pm sd$ results of Expert 1 and Expert 2 were 0.87 ± 0.12 and 0.90 ± 0.2 mm, respectively. In this study for the second set of measurements the results of Expert 1 and Expert 2 were 0.85 ± 0.11 and 0.85 ± 0.17 mm, respectively. It should be noted that direct comparisons between different studies, are difficult, due to the dependence on the measurement protocol, number and type of patients, tissue to be segmented and image quality.

Table 3 showed that the manual measurements of Expert 1 at time 0 versus time 12 months were S, whereas the measurements of Expert 1 at time 0 versus Expert 2 at time 12 months were S for the NP and NS for N. The measurements of Expert 2 at time 0 versus the measurements of Expert 1 and Expert 2 at 12 months and the measurements of Expert 1 versus Expert 2 at time 12 months were all NS. Most of the manual measurements were NS after normalization.

Table 4 showed that NS differences between the manual and the Williams and Shah snakes segmentation method for all manual and automated segmentation cases (NP, DS, N, NDS) were found using the Wilcoxon rank sum test. The smallest HD, (see Table 4), was found between the N-Manual first set NP (3.4), NDS-Manual first set N (4.7), NDS-N (5) and DS-NP (5.2) images, which showed the minimum mismatches between these measurements.

Bland–Altman plots showed (see also Fig. 5) that while all but only a few of the data points lie within two sigma (2σ), of the mean, there was a large spread in the data points. Specifically, for both experts the best plots were obtained for the NDS images, whereas the difference between the segmentation method and the first time manual normalized measurements of Expert 1, was 0.01 mm, and for the second time manual normalized measurements of Expert 2, was 0.09 mm. There was also a negative bias, estimated by the mean difference, which showed that on average the snakes segmentation algorithm overestimates the area relative to normal delineation. The Bland–Altman plots showed that, the best plot was obtained for the NDS images, with smaller differences between experts. The test also showed that the relative differences in IMT values remained constant in all cases, as the IMT increased from 0.4 mm, the lowest, to 1.0 mm, the highest value. Although there was some variability in the measurements of IMT with limits of agreement that ranged from –0.25 to 0.24 mm, with almost all points within these limits. The lower variability was observed for the first time NP manual measurements of Expert 1 and NDS images and for the first time N manual measurements of Expert 1 and NDS images. In [11] the IMT in carotid artery images of sheep was recorded with two different methods, namely by sonomicrometry and by a computerized device. The Bland–Altman plots showed that the difference between both methods followed a Gaussian distribution and the computerized measurements were higher than those of the sonomicrometry. In [30] the limits of agreement reported in IMT measurements between an experience reader and the automated system developed, were better than in this study and ranged from –0.06 to 0.1 mm. The Bland–Altman test was also used in [10] to compare the results of manual and automated detection in myocardial borders, and the segmented border values between manual and automated detection in brachial ultrasound images [28]. Furthermore, the Bland–Altman plot was used in [22], where 24 carotid ultrasound images were analyzed by two experts for validating the results of IMT measurements using a newly developed system by comparing them with those obtained using previous methods and showed no evidence of bias between the two methods.

Some limitations of the proposed method include the presence of acoustic shadowing together with strong speckle noise, which hinders the visual and automatic analysis in ultrasound images. Such images, with bad visual perception, were neither included in this study nor were they delineated by the experts [9, 14, 18–21, 25, 35]. We have also excluded from our segmentation experiments images with extensive echolucency and calcification. This problem is inherent to ultrasound and could be only resolved by using other techniques, like MRI [25]. Backscattered ultrasound is also angle dependent. During the recording of the images a standard recording technique was used to adjust the position of the probe so that the ultrasound beam was at right angles to the arterial wall. This improved the IMC visualization. Moreover, the new spatial compound imaging technique might optimize further carotid plaque imaging [21, 25, 35].

Furthermore, the estimation and positioning of the initial snake contour may sometimes result to segmentation errors. This should be placed as close as possible to the area of interest otherwise it may be trapped into local minima or false edges and converge to a wrong location. In the present study in less than 5% of the cases the positioning of the initial snake contour was not calculated correctly. For these cases the user of the proposed system may run the snake initialisation procedure again in order to estimate the correct initial snake contour. Furthermore, only vessels without atherosclerotic plaques were segmented in this study. The applicability of the proposed snakes border detection in cases where the IMT is larger than 1.4 mm, (see Sect. 2.5 point 8), is not possible. That is because for larger IMT a different initialization procedure, based on plaque segmentation, should be followed as proposed in [20], where the initial contour estimation procedure presented in this study, fails to accurately detect the correct plaque border boundaries.

In this study images recorded from the ATL HDI–3000 scanner were used, although in a recent study [21] it was shown that the ATL HDI-5000 scanner produced better quality images. The reason for using the HDI-3000 images was that because, a complete dataset from the HDI-5000 scanner as well as all IMT measurements were not available, as this scanner was only recently installed. The HDI-3000 dataset was complete and included all patients data, as well as repeated IMT measurements. Additionally, despeckle filtering on N images was not applied in this study, for the manual measurements and the experts only delineated the IMT on the NP and N images. The primary interest of the experts was to investigate the usefulness of normalization in manual delineation. It is therefore our intention to investigate the usefulness of normalisation and despeckling in manual delineation in a future study.

Finally the two experts made some comments for the use of the proposed snake-based IMT segmentation technique and these are summarized below. They were both satisfied from the results, and the easiness of the automated IMT segmentation. The system produced reproducible measurements for both experts and the time of delineation is considerably shorter when compared to the manual. Furthermore, the interaction with the system is minimal. The experts have to select the region of interest and manual correction was required in less than 5% of the cases. More specifically, they were satisfied because the speckle could be reduced prior to the application of the snakes algorithm and thus the visual interpretation as well as the automated performance of the algorithm could be improved. In conclusion they both stated that the system may be used to complement the manual measurements and they were happy to have a system that could reproducibly delineate IMT.

5 Concluding remarks

The IMC snakes segmentation method presented in this paper utilizes and improved snakes initialization and an improved validation of the segmentation method by using despeckle filtering and image normalization. The most important finding of this study is that there was no significant difference of the IMT measurements between the manual and the snakes segmentation measurements. However, when normalization and speckle reduction filtering is applied on ultrasound images of the carotid artery prior to IMT segmentation, the automated NDS measurements are closer to the manual measurements, based on the Bland Altman test, the HD, the CV% and the intra-observer variability.

Furthermore it is noted that better manual segmentation results were also obtained with lower sd, se, CV%, (see Table 2), and good Bland–Altman plot (see Fig. 5), on the manual first set N images when compared with the manual first set NP segmentation results.

The analytical approach of Bland Altman as used in this study, is more appropriate for the evaluation of the consistency of a new method of measurements compared with an established method. Through the use of this approach it was shown that, between the manual first set N measurements and the NDS a small discrepancy, of around 0.05 mm was reported. On this basis the two methods, (manual and snakes segmentation), can be considered interchangeable. However, because the repeatability of the manual measurements, (intra-observer variability), was larger than this of the Williams and Shah snakes segmentation measurements, we conclude that the replacement of the manual with the snakes segmentation system is possible.

Therefore, the pre-processing of ultrasound images of the carotid artery with normalization and speckle reduction, followed by the snakes initialisation and the Williams and Shah segmentation algorithm can be used successfully in the measurement of IMT complementing the manual measurements. It should be furthermore noted that both the manual and the snakes segmentation measurements were performed on linear segments of the carotid artery, because in the clinical praxis the experts are delineating the IMT only in those parts of the vessel where there are no

significant artefacts, signal drop outs and structure irregularities. The validity of the measurements of the proposed methodology can always be easily assessed by the vascular expert. This methodology will be further evaluated on ultrasound images of the carotid collected on a large-scale epidemiological study by our group as well as for the segmentation and measurement of curved segments of the bifurcation or bulb of the carotid artery.

Acknowledgments This work was partly funded through the project Integrated System for the Support of the Diagnosis for the Risk of Stroke (IASIS), of the fifth Annual Program for the Financing of Research of the Research Promotion Foundation of Cyprus 2002–2005, through the project Integrated System for the Evaluation of Ultrasound Imaging of the Carotid Artery (TALOS), of the Program for Research and Technological Development 2003–2005, of the Research Promotion Foundation of Cyprus, as well as, from the Cardiovascular Disease Educational and Research Trust (CDER Trust) UK.

References

1. Abd-Elmonien K, Youssef A-B, Kadah Y (2002) Real-time speckle reduction and coherence enhancement in ultrasound imaging via nonlinear anisotropic diffusion. IEEE Trans Biomed Eng 49(9):997–1014
2. Bland JM, Altman DG (1986) Statistical methods for assessing agreement between two methods of clinical measurement. Lancet 1(8476):307–310
3. Bots ML, Hoes AW, Koudstaal PJ, Hofman A, Grobbee DE (1997) Common carotid intima-media thickness and risk of stroke and myocardial infarction: the Rotterdam Study. Circulation 96:1432–1437
4. Brejl M, Sonka M (1997) Automated design of optimal border detection criteria: Learning from image segmentation examples. In: Proceedings of 19th international conference on IEEE/EMBS, pp 542–545
5. Chalana V, Kim Y (1997) A methodology for evaluation of boundary detection algorithms on medical images. IEEE Trans Med Imaging 16(5):642–652
6. Cheng D, Schmidt-Trucksaess A, Cheng K, Burkhardt H (2002) Using snakes to detect the intimal and adventitial layers of the common carotid artery wall in sonographic images. Comput Meth Prog Bio 67:27–37
7. Cohen I, Cohen LD, Ayache N (1992) Using deformable surfaces to segment 3-D images and inter differential structures. CVGIP Imag Underst 56(2):242–263
8. Cohen LD (1991) On active contour models and balloons. Comput Vis Graph Imag Proces Imag Underst 53(2):211–218
9. Elatrozy T, Nicolaides A, Tegos T, Zarka A, Griffin M, Sabetai M (1998) The effect of B-mode ultrasonic image standardization of the echodensity of symptomatic and asymptomatic carotid bifurcation plaque. Int Angiol 17(3):179–186
10. Jacob G, Noble A, Behrenbruch C, Kelion A, Banning A (2002) A shape-space-based approach to tracking myocardial borders and quantifying regional left-ventricular function applied in echocardiography. IEEE Trans Med Imaging 21(3):226–238
11. Graf S, Gariery J, Massonneau M, Armentano R, Mansour S, Barra J, Simon A, Levenson J (1999) Experimental and clinical validation of arterial diameter waveform and intimal media thickness obtained from B-mode ultrasound image processing. Ultrasound Med Biol 25(9):1353–1363
12. Gutierrez M, Pilon P, Lage S, Kopel L, Carvalho R, Furuie S (2002) Automatic measurement of carotid diameter and wall thickness in ultrasound images. Comput Cardiol 29:359–362
13. Kass M, Witkin A, Terzopoulos D (1988) Snake: active contour models. Int J Comput Vis 1:321–331
14. Kyriakou E, Pattichis MS, Christodoulou C, Pattichis CS, Kakkos S, Griffin M, Nicoliades A (2005) Ultrasound imaging in the analysis of carotid plaque morphology for the assessment of stroke. In: Suri JS, Yuan C, Wilson DL, Laxminarayan S (eds) Plaque imaging: pixel to molecular level. IOS press, Amsterdam, pp 241–275
15. Lamont D, Parker L, White M, Unwin N et al (2000) Risk of cardiovascular disease measured by carotid intima-media thickness at age 49–51: life course study. BMJ 320:273–278
16. Lee J-S (1980) Digital image enhancement and noise filtering by use of local statistics. IEEE Trans Pattern Anal Mach Intell PAMI 2(2):165–168
17. Liang Q, Wendelhag I, Wilkstrand J, Gustavsson T (2000) A multiscale dynamic programming procedure for boundary detection in ultrasonic artery images. IEEE Trans Med Imaging 19(2):127–142
18. Loizou CP, Pattichis CS, Christodoulou CI, Istepanian RSH, Pantziaris M, Nicolaides A (2005) Comparative evaluation of despeckle filtering in ultrasound imaging of the carotid artery. IEEE Trans Ultrason Ferr 52(10):1653–1669
19. Loizou CP, Pattichis CS, Istepanian RSH, Pantziaris M (2004) Intima media segmentation of the carotid artery. IEEE Int X Mediterr Conf Medicon Med Biol Eng POS-03 499:1–4
20. Loizou CP, Pattichis CS, Istepanian RSH, Pantziaris M, Nicolaides A (2004) Atherosclerotic carotid plaque segmentation. In: IEEE 26th Int Conf Proc EMBS, pp 1403–1406
21. Loizou CP, Pattichis CS, Pantziaris M, Tyllis T, Nicolaides A (2006) Quantitative quality evaluation of ultrasound imaging in the carotid artery. Med Biol Eng Comput 44(5):414–426
22. Mancini GBJ, Abbott D, Kamimura C, Yeoh E (2004) Validation of a new ultrasound method for the measurement of carotid artery intima medial thickness and plaque dimensions. Can J Cardiol 20(13):1355–1359
23. Mao F, Gill J, Downey D, Fenster A (2000) Segmentation of carotid artery in ultrasound images: method development and evaluation technique. Med Phys 27(8):1–10
24. Mojsilovic A, Popovic M, Amodaj N, Babic R, Ostojic M (1997) Automatic segmentation of intravascular ultrasound images: a texture based approach. Ann Biomed Eng 25:1059–1071
25. Nicolaides AN, Kakkos SK, Griffin M, Sabetai M, Dhanjil S, Thomas D et al (2005) Effect of image normalization on carotid plaque classification and the risk of ipsilateral hemispheric events: results from the asymptomatic carotid stenosis and risk of stroke study. Vascular 1(4):211–221
26. Otsu N (1979) A threshold selection method from gray-level histograms. IEEE Trans Syst Man Cybern 9(1):62–66
27. Pignoli P et al (1986) Intima plus media thickness of the arterial wall: a direct measurement with ultrasound imaging. Atherosclerosis 74(6):1399–1406
28. Woodman R et al (2001) Improved analysis of brachial artery ultrasound using a novel edge detection software system. J Appl Physiol 91:929–937
29. Selzer RH, Wendy JM et al (2001) Improved common carotid elasticity and intima-media thickness measurements from computer analysis of sequential ultrasound frames. Atherosclerosis 154(1):185–193

30. Stein JH, Korcarz CE et al (2005) A semiautomated ultrasound border detection program that facilitates clinical measurement of ultrasound carotid intima-media thickness. J Am Soc Echocardiogr 18(3):244–251
31. Tegos TJ et al (2001) Patterns of brain computed tomography infraction and carotid plaque echogenicity. J Vasc Surg 33:334–339
32. Trucksaess AS et al (2001) Computerised analysis system using the active contour in ultrasound measurement of carotid artery intima-media thickness. Clin Physiol 21(5):561–569
33. Wang J, Li X (2003) Guiding ziplock snakes with a priori information. IEEE Trans Image Process 12(2):176–185
34. Wendelhag I, Liang Q, Gustavsson T, Wikstrand J (1997) A new automated computerized analysing system simplifies reading and reduces the variability in ultrasound measurement of intima media thickness. Stroke 28:2195–2200
35. Wilhjelm JE, Gronholdt ML, Wiebe B, Jespersen SK, Hansen LK, Sillesen H (1998) Quantitative analysis of ultrasound B-mode images of carotid atherosclerotic plaque: correlation with visual classification and histological examination. IEEE Trans Med Imaging 17(6):910–922
36. Williams DJ, Shah M (1992) A fast algorithm for active contour and curvature estimation. GVCIP Imag Underst 55(1):14–26
37. Xiao G, Brady M, Noble J, Zhang Y (2002) Segmentation of ultrasound B-mode images with intensity inhomogeneity correction. IEEE Trans Med Imaging 21(1):48–57
38. Xu C, Prince J (1997) Gradient vector flow: a new external force for snakes. In: IEEE conf on comp patttern recogn (CVPR'97), pp 66–71
39. Yuen PC, Feng GC, Zhou JP (1999) A contour detection method: initialisation and contour model. Pattern Recogn Lett 20:141–148
40. Zahalka A, Fenster A (2001) An automated segmentation method for three-dimensional carotid ultrasound images. Phys Med Biol 46:1321–1342